






Practical considerations for the harvesting and conditioning of energy from general-purpose teletransmission systems

Kazimierz Kamuda¹, Dariusz Klepacki¹, Oleksandra Hotra²,
Wiesław Sabat¹, Kazimierz Kuryło¹, Janusz Mrocza³, Piotr Kisała²

¹ Department of Electronic and Telecommunications Systems, Rzeszów University of Technology, ul. W. Pola 2, 35-959 Rzeszów, Poland

² Department of Electronics and Information Technology, Lublin University of Technology, ul. Nadbystrzycka 38D, 20-618 Lublin, Poland

³ Department of Control Science and Engineering, Opole University of Technology, ul. Prószkowska 76, 45-758 Opole, Poland

* Corresponding author's e-mail: o.hotra@pollub.pl

ABSTRACT

This paper presents the results of tests of a model semi-passive RFID identifier system from the point of view of efficiency of energy harvesting from teletransmission systems. The previously developed assumptions and guidelines for the concept of implementation of a harvester system applied in individual solutions, as well as the structure of the identifier operation algorithm adopted in these solutions (otherwise known – in the broader meaning of the term – as the scenario of operation of the identifier system) were taken into account in the conducted research. The efficiency of energy recovery and conditioning from electromagnetic environment was verified for the model RFID identifier.

Keywords: energy harvesting, telecommunication systems, energy storage.

INTRODUCTION

The problem of energy recovery from various sources has been widely discussed in recent literature. Initially, this concerned energy recovery was based on mechanical phenomena [1, 2]. Nowadays, electromagnetic waves have also become the subject of interest.

Currently, a worldwide increase in the number of various radio and television communication systems is observed, which is directly related to technological progress. The operation of these systems involves the deliberate emission of electromagnetic energy that transmits useful information (e.g. radio transmitters, television transmitters, data transmission systems, etc.). Nowadays, with the natural electromagnetic environment being heavily polluted, the problem of so-called electromagnetic smog is becoming increasingly important, especially in large urban areas [3].

Such a high level of electromagnetic wave saturation in space has enabled the implementation of a theory proposed at the end of the 20th century concerning the power supply of sensors or electronic biomedical devices [4–9].

Mobile phone systems are a potential source of energy for harvesting. In this context an important parameter characterising both base stations and mobile terminals is the maximum output power of their transmitters. Parameters such as power and emission frequency are precisely defined in the technical specifications of the relevant radio communication systems. The range of electromagnetic fields with limit values generated in the vicinity of base station antennas depends on the power delivered to the antennas and their characteristic of radiation. Under typical operating conditions, electromagnetic field strength levels reaching limit values are observed at distances

not exceeding several dozen metres from the antennas, mainly in the plane of their installation. This distance mainly applies to the area along the main axis of the antennas' radiation [10–13].

Terrestrial television systems, currently implemented mainly in digital technology, are an important part of the electromagnetic environment. In order to maximise the propagation range of the signal, transmitting antennas are usually installed on masts of considerable height above ground level – often exceeding 50 metres – as well as on natural elevations. The permissible values of electromagnetic field strength in the vicinity of radio communication equipment are determined by a number of factors, including the operating frequency of the system, the radiation characteristics of the transmitting antennas, the height of the antennas and, in particular, the effective radiated power (ERP) [14–16].

Another potential source of energy that can be harvested are wireless Wi-Fi telecommunications networks based on the IEEE 802.11 standard, which represents numerous variants, including the most commonly used ones: 802.11a, 802.11b, 802.11g, 802.11n and 802.11ac. The current implementation of the 802.11ac standard enables data transmission at speeds of up to 1 Gbps. This technology uses frequency bands – 2.4 GHz (in 802.11b/g versions) and 5.2 GHz (in 802.11a version) – which requires compliance with strict restrictions on the maximum permissible transmitted signal power. Wi-Fi wireless networks are most often designed for indoor environments, such as buildings, where radio wave propagation is highly complex due to numerous physical obstacles that significantly affect the range and quality of transmission [17–20].

In earlier papers by the authors [21, 22], the results of preliminary studies aimed at understanding the properties of several energy harvesting systems were discussed. There, they were considered as potential energy sources and investigated in terms of their behaviour as a classical power source. Parameters such as the maximum current supplied to the load, source-receiver impedance matching, charging rate and energy conditioning efficiency were considered for potential energy storage in the form of ordinary capacitors and supercapacitors. Such a system should ensure the operation of an identifier (or other energy receiver with characteristics similar to the model identifier, in particular in terms of the time schedule of the energy storage – power

supply mode of the receiver) in terms of energy acquisition and retention (under specified field conditions) from common-use telecommunications systems available in the area with adequate transmission and energy capabilities and a specified time-functional regime.

The results presented in this paper are an extension of the research undertaken in previous stage, allowing the detailed configuration guidelines and the area of correct system operation to be established under conditions connected with the real one for the model demonstrators of semi-passive identifiers. This required the determination and verification of the parameters and the possibility of its interaction with the other system components under the specific loading conditions of this specific energy source with a load of a very unusual character. The determination and verification of the parameters particularly concern the quality of the energy conditioning process and the possibility of storing energy within the optimal range of efficiency and effectiveness of these processes. Verification of the energy balance is an unequivocal criterion for the probability of ensuring correct operation of the identifier under specific environmental conditions, taking into account the configuration of system parameters affecting this balance (DC/DC converter thresholds, hysteresis keys, system timing, etc.).

MATERIALS AND METHODS

Test setup

In the solution developed and tested as part of the work (Figure 1), which is an integrated semi-passive identifier, the key system to ensure its autonomy is the electromagnetic field harvesting module. To establish the operating conditions, it was assumed that GSM900 would be used as the test telecommunications system. This is still the most popular and generally available mobile phone standard, operating simultaneously in frequency bands with relatively good propagation conditions. In the course of the investigation, a number of test versions of the model identifier system with the power supply under test were verified, the configuration of which was modified as the research progressed. Each solution includes an external or integrated harvester antenna with an operating bandwidth from 930 to 975 MHz.

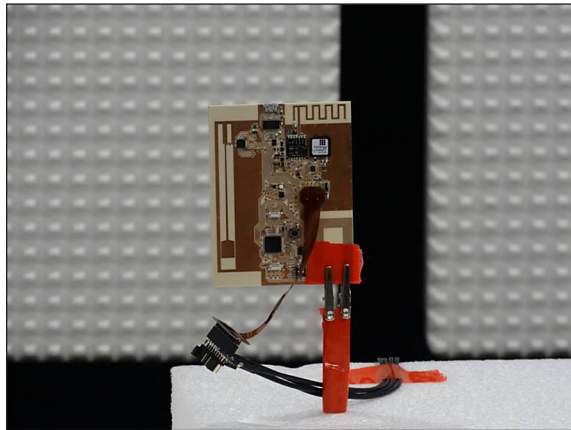


Figure 1. View of one of the test versions of the semi-passive identifier demonstrator (concept 1 – version without solder mask) on the test stand

Depending on the version, the P2110B chip from Powercast or the P21XXCSR developed by the authors in collaboration with Powercast was used as the harvester circuit in the energy recovery and storage system, as discussed in earlier studies. It is a universal chip designed to operate at frequencies from 824 to 2495 MHz in several sub-bands (Table 1), which allows the parameters of the harvester system to be verified in real conditions also in a wide range of potential energy harvesting sources (GSM, DCS, UMTS, Wi-Fi bands). In version 2 it is attached to the system as an additional external module. Both test modules are equipped with additional circuit solutions implementing alternative mechanisms to improve the efficiency of the main inverter.

The demonstrator circuit was designed on the basis of the analyses and solutions proposed, performed and studied in the previous research, considered in relation to the electronic design of the identifier circuit. To facilitate the analysis of the obtained results, the proposed block-functional diagram of the identifier is presented in Figure 2.

The energy extracted from the harvesters is stored in a CP capacitor. The electronic circuits are protected against an uncontrolled voltage increase on this capacitor above 4.1 V, which could be dangerous for some semiconductor circuits. For a voltage V_{CP} of less than 2.4 V, the current leakage is of the order of 300 pA (generated by the TS12001 protection comparator circuits). This represents a negligible load and allows energy to be stored efficiently from sources with even minimal efficiency. If the voltage value on the capacitor V_{CP} exceeds 1.9 V, it is possible to supply the RFID interface and harvester operating circuit – M24LR16E and correct communication with the reader-programmer appears. This can appear very quickly due to the negligible power consumption of the other circuits of the identifier. A further increase of V_{CP} beyond 2.4 V will cause comparator 1 to switch on and energy will flow to the CRTC capacitor until V_{CP} drops to 1.9 V and the comparator 2 circuit goes into an off state. In order to avoid feedback of energy from the capacitor (and not to use the additional diode shown symbolically in the block diagram, causing significant energy loss in the circuit), an additional switch circuit was used with a DG4157 key, controlled by the above-mentioned comparator. The low turn-on resistance of the key causes negligible losses and almost all energy is transferred to the CRTC capacitor. When it is switched off, the very low leakage current of its output effectively limits unwanted energy drain from this capacitor and extends the operating time of the RTC itself. By appropriately selecting the capacitance of the CP and CRTC, it is possible, as a result of a single charge to the CRTC capacitor, to obtain enough voltage on it to run the RTC circuit and the control microcontroller.

If the recovered energy is sufficiently high, the voltage on the CP capacitor will increase despite the 2 V comparator circuit being switched

Table 1. Operating frequencies of Powercast Corporation's P21XXCSR harvester system, developed in collaboration with Elmak Corp. (concept 2)

Component	Band	Band (MHz)	Center frequency (MHz)
J1	GSM-850 uplink	824–849	836.5
J2	Europe RFID and GSM-850 downlink	865–894	879.5
J3	GSM-900 and EGSM-900	925–960	947.5
J4	GSM-1800 uplink	1710–1785	1747.5
J5	GSM-1800/LTE downlink	1805–1825	1815
J6	WiFi 2.4 GHz (ETSI)	2400–2495	2442

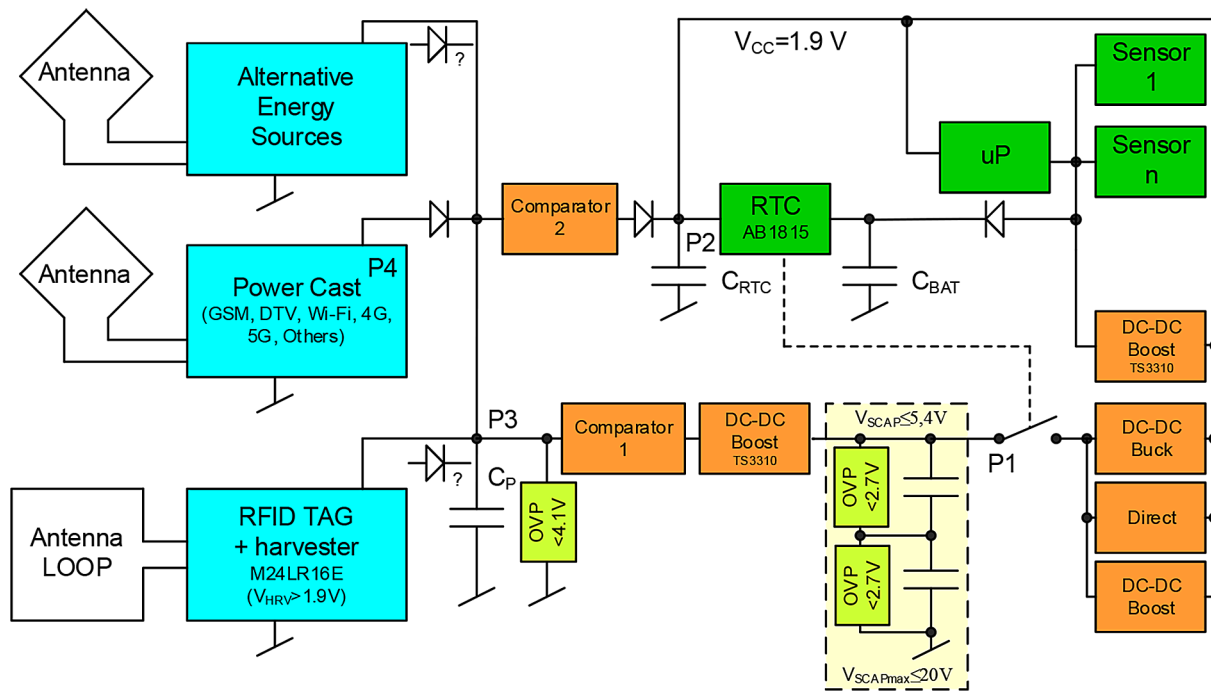


Figure 2. Simplified block diagram of the energy conversion and power system of the systems in the model identifier (concepts 1 and 2)

on. This has been anticipated and, once the voltage reaches 2.5 V, comparator circuit 1 will be switched on. Adequate capacitance at the input allows the TS3310-based Boost converter to start easily and begin charging the supercapacitors with the excess energy recovered. The $C_{(SCAP)}$ supercapacitors are the main energy storage. The authors' experience shows that using a higher voltage capacitor bank allows the stored energy to be more easily managed, so the circuit uses a series connection of two supercapacitors. The maximum voltage is 5.2 V. To ensure that the two stores are charged evenly and to avoid the use of a so-called balancer, the model uses a circuit to prevent the voltage rising above a safe value on the individual supercapacitors, built using 2.7 V comparator circuits on each supercapacitor. Minimising the switching hysteresis of the TS12001 circuits from the original value of 0.5 V to around 0.1 V significantly reduces the individual supercapacitor discharge due to exceeding the maximum voltage.

Activation of the AB1815 real-time clock circuit will occur when the voltage value of 1.6 V on capacitor C_{RTC} is exceeded. This circuit determines the operation of the identifier. Firstly, it determines the moments when the microcontroller is switched on and the defined tasks are executed (implementation of the operating scenario).

Secondly, if the voltage on C_{RTC} drops to a value below 1.6 V (in the absence of recharging by the energy acquisition circuits due to the need to perform/complete the tasks defined in the scenario), it will initiate the process of recharging the C_{RTC} capacitor with the energy stored in the energy storage. The activation of the circuits associated with the above-mentioned functions is performed by an additional switch circuit with a DG4157 key. It is controlled via the corresponding output of the RTC circuit. Its activation therefore charges the capacitors connected to the main power supply line (1.9 V) and starts the microcontroller.

The microcontroller chip (C8051F902) is configured to operate from as low as 0.9 V (thanks to the built-in step-up converter), allowing it to operate correctly under such extreme conditions of energy supply from the C_{RTC} capacitor. In parallel, an inverter (TS3310) configured to obtain an output voltage of 5 V is activated, enabling, with a large energy supply, all the identifier's circuits and sensors to be powered. The use of comparators allows the switching voltages of the operation of the individual branches to be accurately selected. The availability of control signals in the individual voltage ranges makes it possible to control the sleep states of the converters. The control system also constantly selects the most favourable ways of

maintaining the required energy level in the C_{RTC} condenser, which supplies the RTC itself and is key to the reliability of the entire system.

The microcontroller chip is only switched on by the RTC clock according to a predetermined schedule of system operation, known as an identifier operating scenario. If the reason for switching on the microcontroller was to perform the relevant tasks, the microcontroller performs certain configuration processes before this activity. Since each component of the system (sensors, memories, etc.), powered via an appropriate key, power consumption can be largely controlled by switching on only the systems currently in use. The power supply of the I2C serial bus pull-up resistors, which are only switched on during transmission, is also implemented in the same way.

According to these assumptions, a complete electronic circuit for a demonstrator of an autonomous RFID tag in the HF band with energy harvesting from the electromagnetic field of the RFID system, other telecommunication systems (ambient energy) or the aforementioned alternative sources of energy harvesting was designed and made. The system cooperates with a temperature and humidity sensor and has the possibility of attaching another two sensors (meeting the requirements of their integration into the board system) of any physical or chemical quantities. This increases the flexibility of the system and allows the system to be tested for preferred individual applications. Interestingly, for the purposes of future tests under target conditions, a measuring system has also been developed, which allows autonomous measurements of selected values of voltages and currents in the identifier system, in order to facilitate testing of the system in the field, without the need for specialised measuring equipment. The measurement system, made in the form of an overlay on the base module, is powered from an additional external source and equipped with an operator panel to facilitate measurements and data acquisition outside the laboratory (the mobile measurement overlay with display and external power supply, placed on the board in concept 2 – Figure 3).

Finally, a test stand was proposed to simulate the operation of an identifier operating with a variable load attached from time to time (Figure 4). It consists of a model energy conversion and storage system, a specially designed controlled load, a USB 1608GX measurement card from the Measurement Computing Corporation,

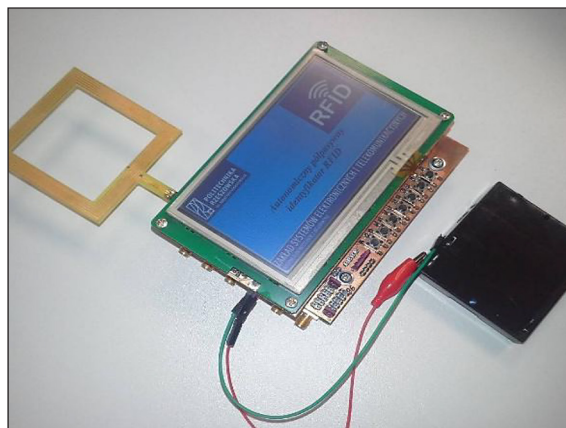


Figure 3. View of the complete demonstrator circuit and the attached example of the external antenna of the RFID system

a regulated power supply, a computer with LabView software installed and a digital oscilloscope used to control the timing parameters. A block diagram of the measurement system is illustrated in Figure 5.

METHODOLOGY

Measurements were carried out in the TDK anechoic chamber available at the Electromagnetic Compatibility Laboratory of the Department of Electronic and Telecommunications Systems of the Rzeszów University of Technology in systems analogous to those discussed in earlier studies [21, 22].

The study employed a collection of devices designed to generate electromagnetic fields for testing immunity to electromagnetic radiation, along with probes to measure field strength, and systems that facilitated the implementation and automation of remote measurements of parameters critical to the research. A set of absorbers was installed on the floor of the anechoic chamber to capture radiation reflected from that part of the room. For the measurements, a specially developed method was used to determine the electric field strength, relying on the symmetry of the radiation pattern of the transmitting antenna. This approach enabled simultaneous measurement and powering of the energy harvester system while minimising any mutual interference affecting the field strength readings.

Rohde and Schwarz's EMS_1GHz and EMS_6GHz system devices were used in the tests. Most of the equipment is housed in measurement

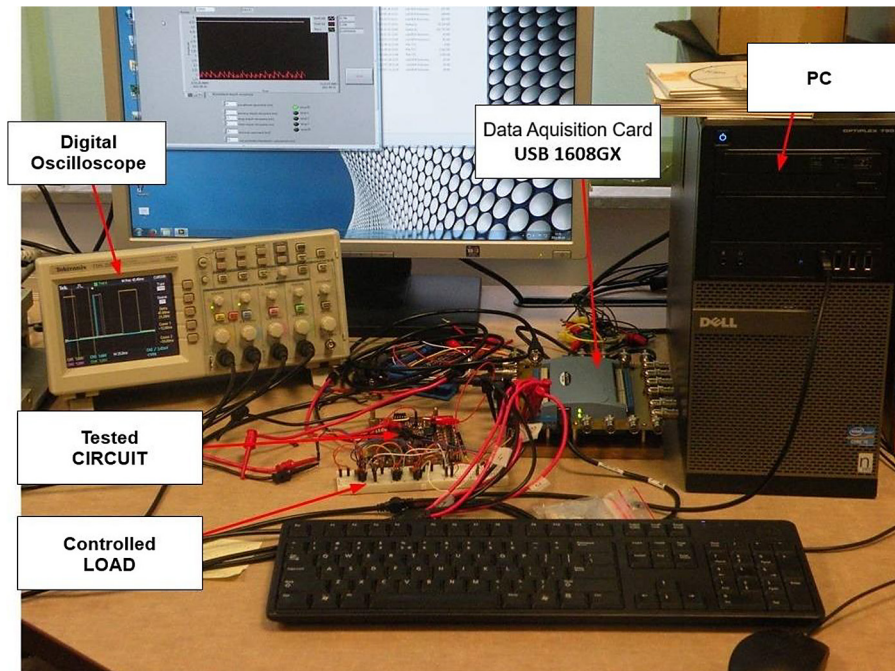


Figure 4. Measurement stand for testing the identifier operating scenario

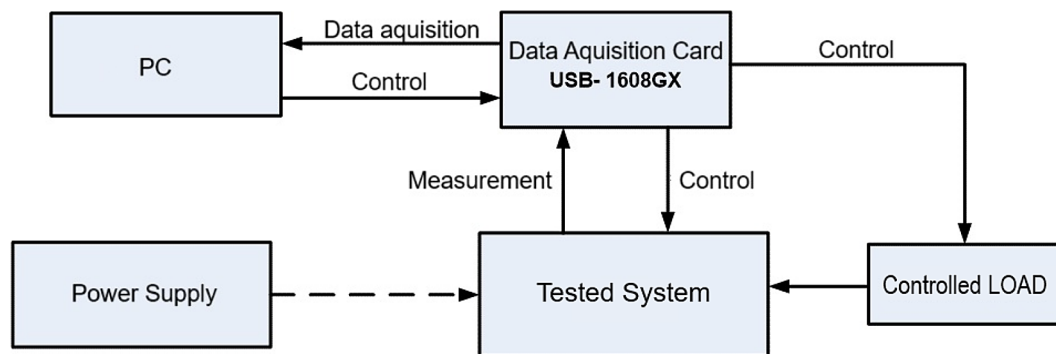


Figure 5. Block diagram of the test stand

racks, permanently placed in the amplifier room next to the anechoic chamber. The 1_GHz type system consists of an SMB 100A generator, a BBA 100 power amplifier, an NRP2 power meter with NRP-Z11 measurement probes from Rohde and Schwarz and an HL233 antenna located in the chamber. The second system is respectively composed of an STLP9149 antenna, an SMF 100A generator, an NRP2 power meter from Rohde and Schwarz and a BLMA1060-100/100/50D amplifier (from Bonn).

The HI6005 probe from ETS-Lindgren was used to measure the intensity of the generated electromagnetic fields (electric field). This probe is capable of measuring electric field strengths in the frequency band from 100 kHz to 6 GHz with a dynamic range of 0.5 V/m to 800 V/m.

The complete test stand in the anechoic chamber and schematic diagram for adopted concept of measuring field distribution are presented in Figure 6.

The operation of the system is controlled by Rohde and Schwarz's EMS32 application, used in this case to set parameters and stabilise the electric field. The HI 6105 probe is placed in a feedback loop. The identifier under test is placed symmetrically to the probe with respect to the antenna axis. The test system, the field strength can be simultaneously controlled and the identifier parameters can be measured under the set conditions. As standard, it is used for tests performed in an EMC chamber, in accordance with the relevant standards [23]. After appropriate modification of the settings of this

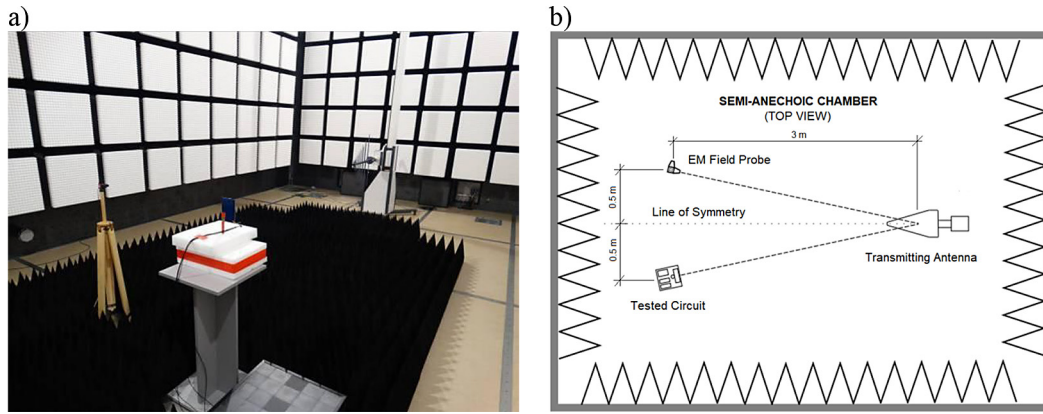


Figure 6. Test stand for the analysis of the electric field strength distribution (power density) in an anechoic chamber: a) stand with the HL233 antenna as the source of the electromagnetic field, b) schematic diagram for adopted concept of measuring field distribution

package, it was possible to effectively conduct the described tests with the possibility of automatic stabilisation of the set field strength, regardless of the bandwidth, signal frequency and antennas used [21, 22].

The test circuits were made with and without a solder mask. LVH-900 Mechanic (UV Curing Solder Mask Ink) was used as the solder mask. It is worth noting that for research purposes, the thickness of this layer was increased to 70 μm to determine the effect of this parameter on energy harvesting.

During testing of the version 1 demonstrator system (in versions with and without solder mask), different locations of the system relative to the transmitting antenna were analysed to take into account the polarisation and alignment of the main harvester antenna beam relative to a potential RF signal source. The demonstrator positions practically verified during the tests are shown in Figure 7.

Version 2 of the identifier chip was tested together with an evaluation chip supplied by the harvester manufacturer – Powercast Corporation. This was possible because the identifier circuits were designed as modules, attached to the harvester circuit in a sandwich type arrangement. Selected parameters of the antenna used in the tests are summarised in Table 2. It also allows possible measurements to be made in all bands in which the tested harvester system, and thus also the model identifier system, can operate.

Under laboratory conditions, the voltage and currents at the test points were measured using a four-channel remote analogue data acquisition module type NI 9222 from National Instruments with a sampling frequency of 500 kS/s and a resolution of 16 bits. The module was placed in a chamber in a suitably shielded box, and by using control and data reading via an optical USB connection, the influence of the measurement system on the measurement results obtained was minimised.

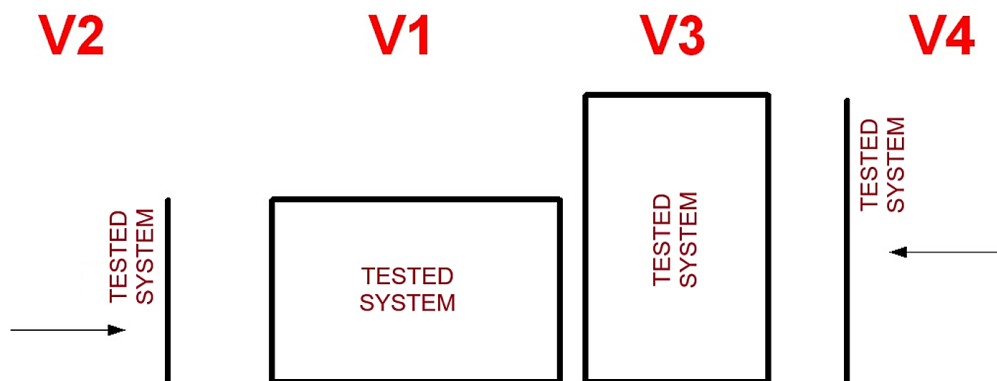



Figure 7. Schematic presentation of the positions of the demonstrator analysed during the tests in relation to the transmitting antenna of the test system

Table 2. View and electrical parameters of the PE51054 Pasternak antenna used in the testing of the Powercast Corporation’s P21XXCSR harvester [24]

Parameters: Characteristics: directional Vertical polarisation V Frequency range: 806–960 MHz and 1710–2500 MHz Energy gain: 7 dBi Radiation angles: Plane V: 47° Plane H: 88 ° VSWR: < 1.5:1 Sizes (W H×× D): 210 × 180 × 44 mm Weight: 470 g	
---	--

RESULTS AND DISCUSSION

Experimental results

As a first step, version 1 of the demonstrator system was tested. First, the voltage obtained in the harvester system of the tested system was checked for the selected electric field strength. On the basis of previous measurements of real field strengths around the transmitting stations of general-purpose teletransmission systems, a value of 3 V/m was selected to be obtained continuously at least at selected fixed locations. Since, by definition, the model system in this version was intended to operate in the frequency range of the GSM system bands, it was of most interest to obtain an answer to the question of whether the resultant operating frequency of the antenna and the harvester system would reflect the assumptions made during system design. An additional element requiring examination was the introduction of an additional technological layer to the identifier in the form of a solder mask with parameters significantly different from those assumed (the influence of the technological process of the company making the customised test circuit boards). Therefore, two versions were tested: both the version with the solder mask and the one without the protective layer. The results of these tests are presented in Figures 8 and 9. The designations V1 to V4 refer to the above-described placement of the demonstrator relative to the test system’s transmitting antenna. Comparing these waveforms clearly shows a shift of the maxima in the solder

masked system towards frequencies outside the bandwidth of the European version of the GSM system, especially for the energetically attractive positions V3 and V4 of the demonstrator. This raises the need for special care in terms of the solder mask design and the care taken in the execution of this PCB circuit layer in applications with harvester circuits, as is the case with classical RF circuits.

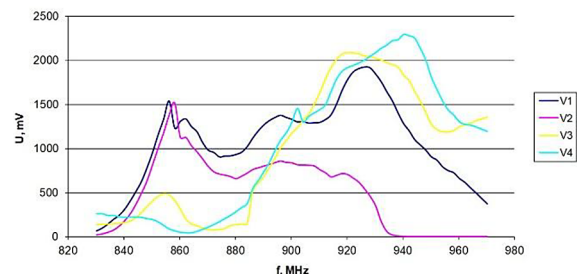


Figure 8. Output voltage dependence of the demonstrator harvester system version 1 for a system without solder mask ($E = 3 \text{ V/m}$)

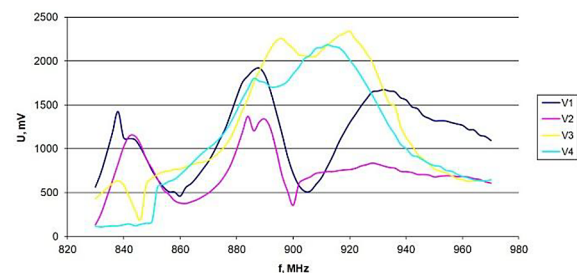


Figure 9. Output voltage dependence of the demonstrator’s version 1 harvester system for a solder masked system ($E = 3 \text{ V/m}$)

Aware of the limitations of the frequency range of the harvester-antenna system, the dependence of the output voltage of this system as a function of frequency was investigated for different electromagnetic field strengths. Only those locations of the demonstrator system in relation to the transmitting antenna, which appeared to be the most favourable in terms of the output voltage, were selected for testing. The results of these measurements are presented in Figures 10 to 13.

Based on the analysis of these data, it can be seen that, in each case, the field strength of the electromagnetic field from a potential energy recovery source at the identifier location point must be greater than 1.5 V/m when considering the operation of the system in the frequency band dedicated to the GSM system. Paradoxically, the solder masked circuit board shows a higher energy harvesting efficiency, but unfortunately in the band it offers it is difficult to expect possible strong signal sources with a power density sufficient to achieve the minimum required output voltage level.

In order to ascertain the actual minimum field strength to be ‘recovered’ to trigger the energy conditioning and storage system, a series of further tests were carried out.

For the operating band of the identifier in version 1, the field strength of the source was altered to achieve the effect of the input circuit inverter starting up and ensuring continuous energy transfer to the storage. It was assumed that continuous, stable operation of the inverter would mean achieving the required minimum field strength. Figures 14 and 15 show the obtained results. As can be seen from these figures, the minimum field strength to maintain operation of the energy storage system oscillates around a value of 2 V/m. Interestingly, the most favourable result was achieved at frequencies in the lower range of the

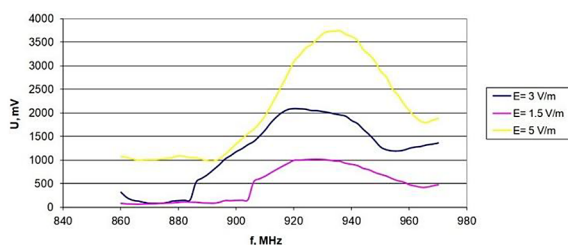


Figure 10. Dependence of the output voltage of the demonstrator’s version 1 harvester circuit on frequency for a circuit without solder mask and a V3-type arrangement

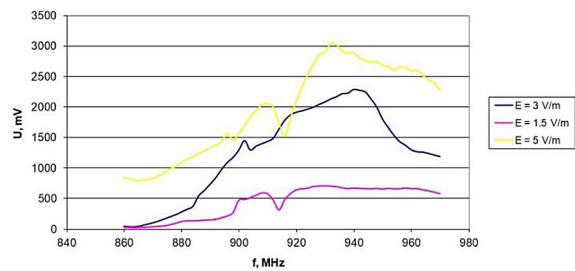


Figure 11. Dependence of the output voltage of the demonstrator’s version 1 harvester circuit on frequency for a circuit without solder mask and a V4-type arrangement

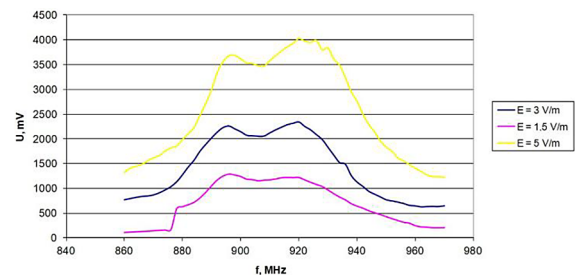


Figure 12. Dependence of the output voltage of the demonstrator harvester system version 1 on frequency for the system with solder mask applied and type V3 arrangement

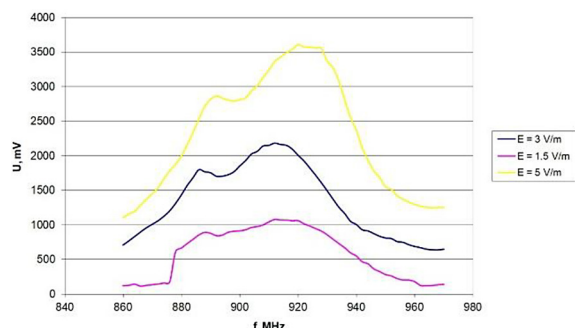


Figure 13. Dependence of the output voltage of the demonstrator’s version 1 harvester system on frequency for the system with solder mask applied and V4-type arrangement

GSM down-link band using location V1. From 950 MHz onwards, locations V3 and V4 already perform more favourably.

At the end of this part of the research, an attempt was also made to evaluate the performance of the energy storage system and the time required to reach a state where the actual identifier system could be activated and start working. Figures 16 and 17 present example results. Analysing the case with the V1 location at a

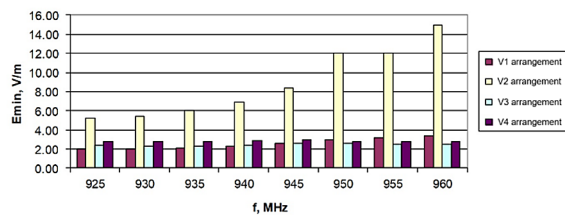


Figure 14. Minimum electromagnetic field strength at the tag placement point for a solder mask-free circuit

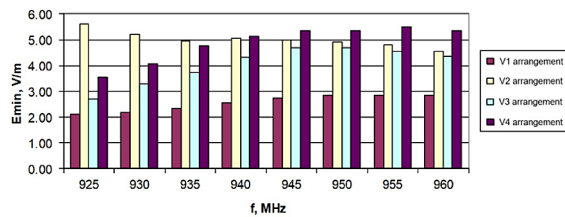


Figure 15. Minimum electromagnetic field strength at the tag placement point for a solder masked chip

frequency of $f = 925$ MHz, which, according to previous results, guaranteed the start of the conditioning and energy storage system at the minimum field strength, it can be concluded that, for a field strength of 3 V/m, the time to reach a voltage of 2 V on the supercapacitor was about 3300 s for the solder masked system and about 3000 s for the system without solder mask. This is interesting, as previous studies have shown a difference in minimum field strength of approximately 0.1 V/m

It should be stressed that this type of research is very time-consuming and each measurement cycle is counted in hours. This is due to the small amount of energy that can be extracted in this way and the enormous capacities of modern supercapacitors used as energy storage in model systems.

As the electromagnetic field strength increases, this time is reduced, but these changes are relatively small and do not significantly reduce the measurement cycle time.

For proper operation of the identifier system, it is important to have stable conditions of energy extraction that can guarantee certainty of accomplishing the tasks assigned to such a system. Therefore, the installation of an identifier in a specific application should be preceded by at least simplified measurements of the achievable energy densities (field strengths) and, if possible, an indication of the most favourable antenna system orientation in terms of energy.

In the second stage of the research, tests were also carried out on version 2 of the identifier. The main focus was on verifying the ability of the energy harvesting system to feed the identifier systems and to store energy in the internal storage. The tests were carried out in a model system fed from the wideband PE51054 antenna from Pasternack used in the P21XXCSR harvester tests for frequencies 836.5 MHz, 879.5 MHz and 947.5 MHz, which are the centre frequencies of the bands operated by the above harvester system in the range up to 1 GHz.

Firstly, the influence of the electric field strength of the analysed common-use teletransmission system was studied for the adopted frequencies. Voltages at four test points of the system were monitored (see Figure 2):

- P1 – output voltage of the main inverter of the identifier system, which is also the voltage at the terminals of the main energy storage
- P2 – energy storage voltages of the RTC power supply;
- P3 – collective energy storage (capacitor) for all energy harvesting systems;

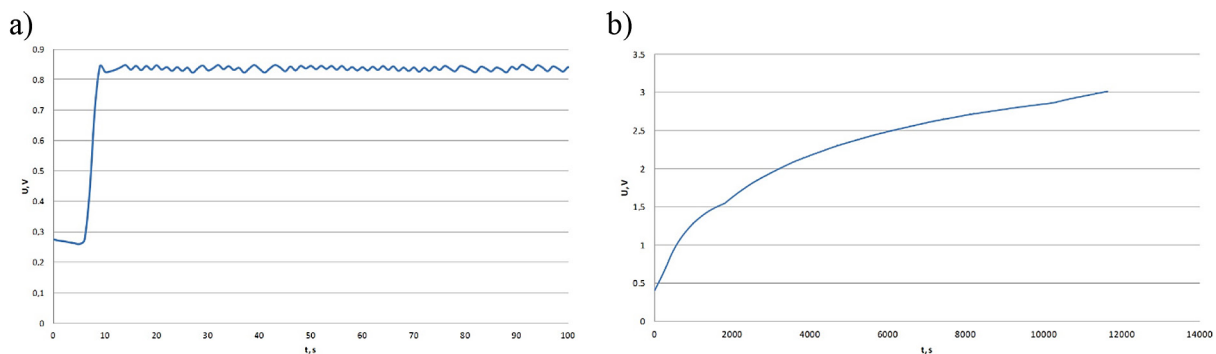


Figure 16. Inverter operation (a) and energy storage charging curve (b) at 925 MHz and for an electromagnetic field strength of 3 V/m in a solder masked system at location V1

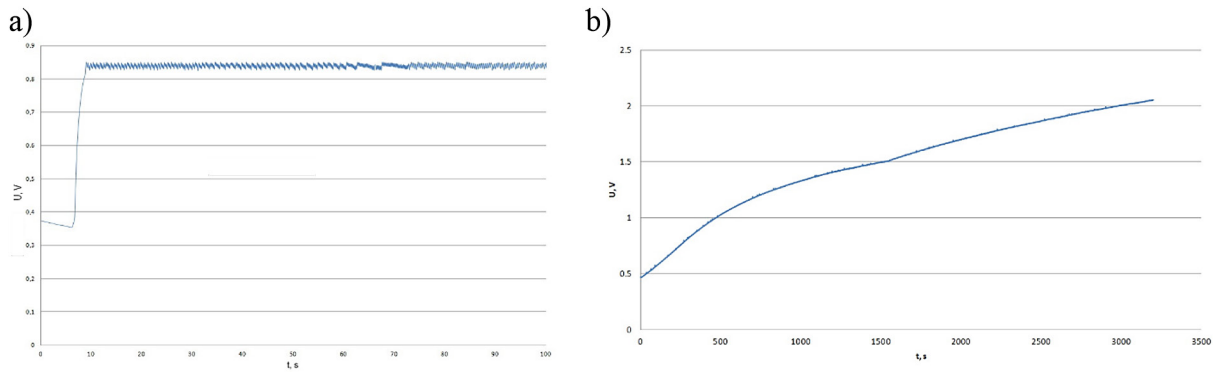


Figure 17. Inverter operation (a) and energy storage charging curve (b) at 925 MHz and for an electromagnetic field strength of 3 V/m in a system without solder mask at location V1

- P4 – harvester system output voltage obtained at the terminals of the harvester intermediate energy store (capacitor limiting the frequency of activation of the input converter).

As mentioned, the design was guided by the idea of redundancy of the power path of the microprocessor controlling the operation of the identifier model, allowing it to be activated both from the main energy storage (normal operation) and on an ad hoc basis from the RTC clock storage when triggered by this system in the absence of sufficient energy in the main storage. Two solutions were investigated in parallel: operation of the identifier model's built-in inverter fed directly from the harvester's output, or stand-alone operation of the Powercast module's inverter – with the aim of selecting a better – especially in terms of conversion efficiency – inverter system.

Figures 18 to 27 show the results of testing the model system in implementation 2 for frequencies of 836.5 MHz, 879.5 MHz and 947.5 MHz. For the frequency of 836.5 MHz, measurements were performed for the two versions of the input converters according to the above assumptions.

The results clearly indicate that it is more efficient to use only the model-developed voltage converter. Comparing, for example, Figures 18–21, it can be seen that the Powercast inverter, when operating at a much higher frequency resulting from a smaller discrepancy in the operating voltage thresholds (e.g. 1–1.25 V), causes a significant decrease in its conversion efficiency. This results in a reduction in the voltages obtained at individual points in the circuit, i.e. a resultant drop in the efficiency of the entire identifier circuit. Similarly, this can be seen in other cases (Figures 22–25), even for sufficiently high

electromagnetic field strengths. In the other cases, trends similar to those observed for the harvester system itself emerge from the measurements. This is understandable insofar as the efficiency of energy recovery as measured by the magnitude of the output voltage depends mainly on the characteristics of the antenna-harvester system (Figures

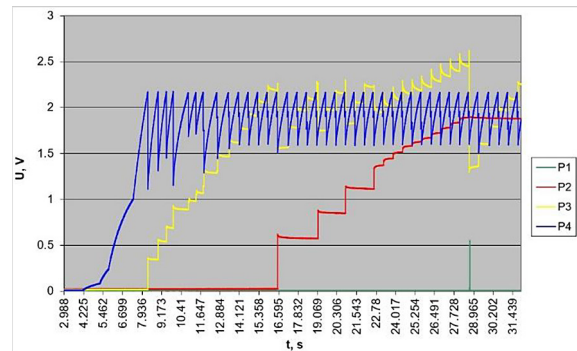


Figure 18. Voltage waveforms at test points of the demonstrator system at 836.5 MHz at a field strength of 1.2 V/m – model system inverter

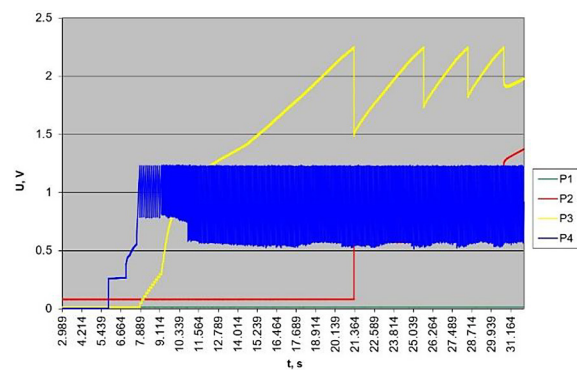


Figure 19. Voltage waveforms at test points of the demonstrator system for 836.5 MHz at a field strength of 1.2 V/m – Powercast's own inverter

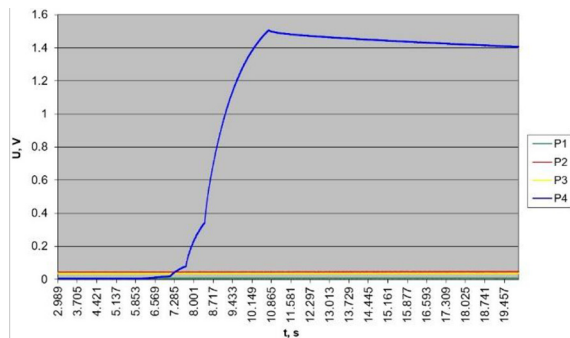


Figure 20. Voltage waveforms at test points of the demonstrator system at 879.5 MHz at a field strength of 1.2 V/m – model system inverter

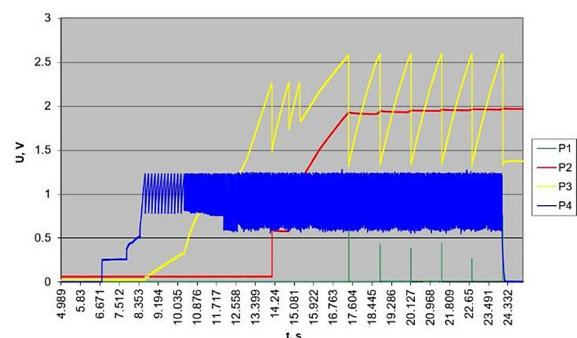


Figure 23. Voltage waveforms at test points of the demonstrator system for 836.5 MHz at a field strength of 3 V/m – Powercast's own inverter

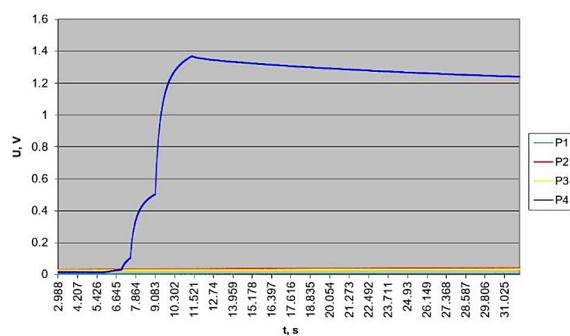


Figure 21. Voltage waveforms at test points of the demonstrator system at 947.5 MHz at a field strength of 1.2 V/m – model system inverter

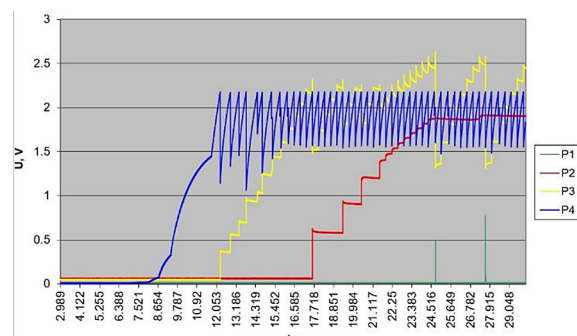


Figure 24. Voltage waveforms at test points of the demonstrator system at 879.5 MHz at a field strength of 3 V/m – inverter of model identifier system

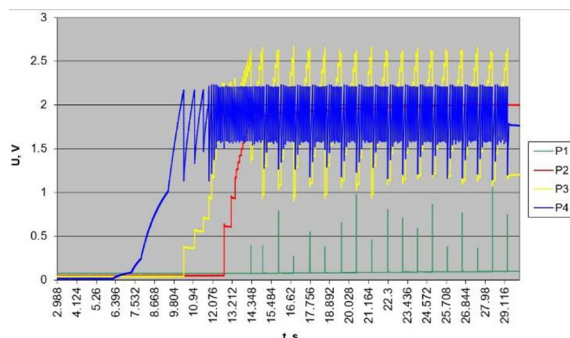


Figure 22. Voltage waveforms at test points of the demonstrator system at 836.5 MHz at a field strength of 3 V/m – model identifier system inverter

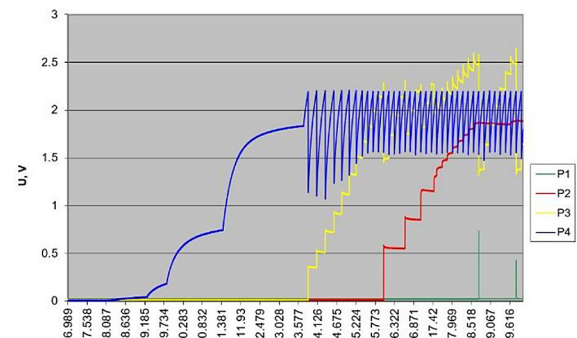


Figure 25. Voltage waveforms at test points of the demonstrator system at 947.5 MHz at a field strength of 3 V/m – inverter of model identifier system

26–29). In the analysed cases, voltages obtained differ from those for the harvester alone due to the actual loading of this system with a certain internal impedance that varies with the operating conditions. It can be seen that for all tested frequencies, the limit of correct operation of the model identifier with the Pasternack antenna is the electric field strength level of 3 V/m (the

correct operation of the system was considered to be the appearance of impulses charging the energy storage, which guarantee that after some time the appropriate voltage is obtained at the main energy storage, or – alternatively – the voltage at the hand-held RTC clock storage).

Figure 30 shows the charging curves of the main energy storage obtained at 1200 s for the

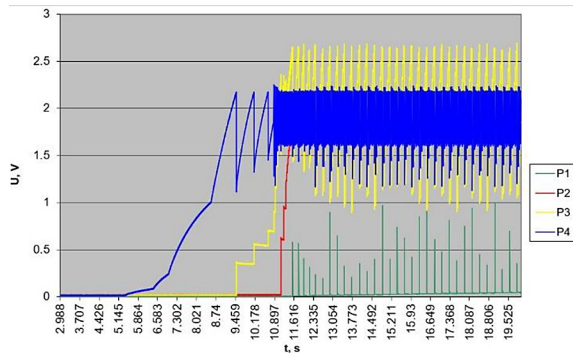


Figure 26. Voltage waveforms at test points of the demonstrator system at 836.5 MHz at a field strength of 5 V/m – inverter of model identifier system

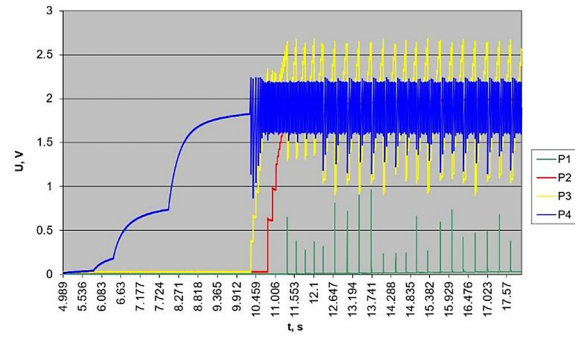


Figure 29. Voltage waveforms at test points of the demonstrator system at 947.5 MHz at a field strength of 5V/m – inverter of model identifier system

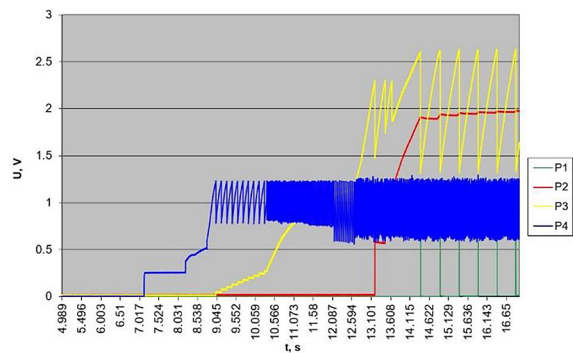


Figure 27. Voltage waveforms at test points of the demonstrator system for 836.5 MHz at a field strength of 5 V/m – Powercast's own inverter

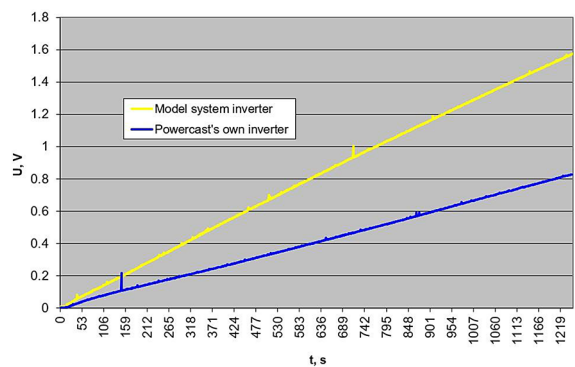


Figure 30. Example energy storage charging curves for the harvester model system inverter and Powercast's own inverter in the demonstrator test system for a frequency of 836.5 MHz at a field strength of 3 V/m

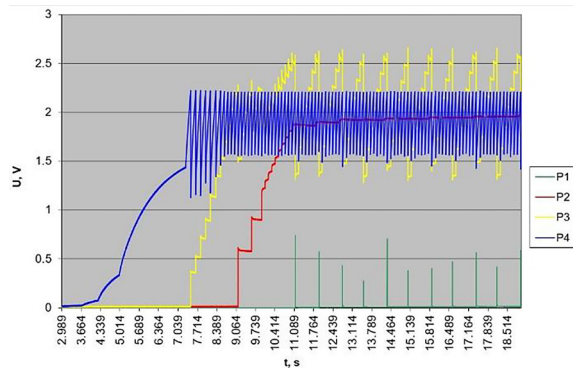


Figure 28. Voltage waveforms at test points of the demonstrator system at 879.5 MHz at a field strength of 5 V/m – inverter of model identifier system

alternative inverter case of the harvester system discussed above. As can be seen, the system with its own inverter obtained almost twice the voltage on the main energy storage. This may be of considerable importance in real-life applications of the demonstrator system in cases of lower values of available power density.

The harvester systems (Powercast, RFID HF and possibly others) charge the capacitor of the main energy store with the acquired energy. In the solution of the autonomous identifier version 2, which cooperates with the Powercast harvester circuit as its extension (overlay), it is possible for the two circuits to cooperate in yet another way. In the identifier circuit itself, it is possible to directly measure the parameters of the energy recovered from the selected frequency band in the Powercast circuit (before the inverter). In addition, a TS3310 inverter circuit is implemented in the identifier circuit, which can cooperate with the selected energy harvesting circuit in the Powercast circuit. This allows two frequency circuits of the Powercast circuit (out of six available) to operate in parallel – one circuit via the on-board inverter in the Powercast circuit, the other via the TS3310 inverter implemented in the model. Both circuits

charge the main energy storage capacitor with the acquired energy.

The measurements carried out clearly confirmed the superior performance of the proposed solution with respect to that offered by the embedded converter circuit in the Powercast solution. It would be reasonable to use TS12001 circuits at a lower voltage than 1.7 V, which would allow the converter to operate at a lower voltage at the output of the Powercast rectifier circuit, i.e. in a lower electromagnetic field, but, on the other hand, a significant reduction in this voltage leads to worse starting conditions for the converter, which may reduce the efficiency of the energy conversion.

Criteria for determining the operating scenario of the system

A very important component of the identifier circuit is the main energy storage (supercapacitor), which is the main element responsible for storing an adequate amount of energy. The use of a supercapacitor seems to be a good solution due to the long service life of this type of component. Although this was not investigated in this study, it is assumed that a typical supercapacitor should withstand approximately 500,000 charge and discharge cycles. This is a much better result than conventional batteries. In order for the identifier to operate correctly, it is important both to select the supercapacitor properly, as well as to define the conditions for its correct operation and to select the right circuits to use the stored energy in the most efficient way possible. To this end, load tests were carried out on the developed identifier, taking into account the stabilisation of the supercapacitor voltage at an assumed level, guaranteeing, on the one hand, the reliability and, on the other, the safety of the system and the cooperating elements connected to it. Such elements may be, for example, various types of sensors, which are connected to the identifier from time to time (in accordance with the assumed scenario and the possibility of their power supply) and are also an additional load for it.

When analysing the possible operating scenarios of an identifier with additional circuits attached to it, a great many cases can be considered. A special case occurs when the identifier with the attached sensor can only operate using the energy previously stored in its internal storage (supercapacitor). This is the worst case because operation

of the system will only be possible until the energy stored in this storage is exhausted.

Before each measurement, a full charge of the supercapacitor takes place. Once C_{SCAP} has been charged to its rated voltage, a cyclic load is applied to the system under test. The storage system and the effect of its load were tested with both an integrated output converter and a linear stabiliser with an output voltage of 1.9 V (see Figure 2). The task of these circuits is to match the voltage at the terminals of the supercapacitor to a value suitable from the perspective of supplying the output circuits.

The load was constructed using Vishay Siliconix's SIP 32431 high-speed switches (Figure 31) and resistances with specific values attached in parallel using these circuits (Figure 32). These were selected in terms of the required values of the currents flowing in the circuit depending on the required operating conditions. The connection of the individual load branches to the circuit under test, according to a predetermined sequence, was carried out using a Measurement Computing USB 1608GX card. The measurement card also made it possible to record the measured values of the supercapacitor voltage and the voltage on the load. The operation of the USB-1608GX card and the acquisition of measurement data was realised using an application developed in the LabView environment.

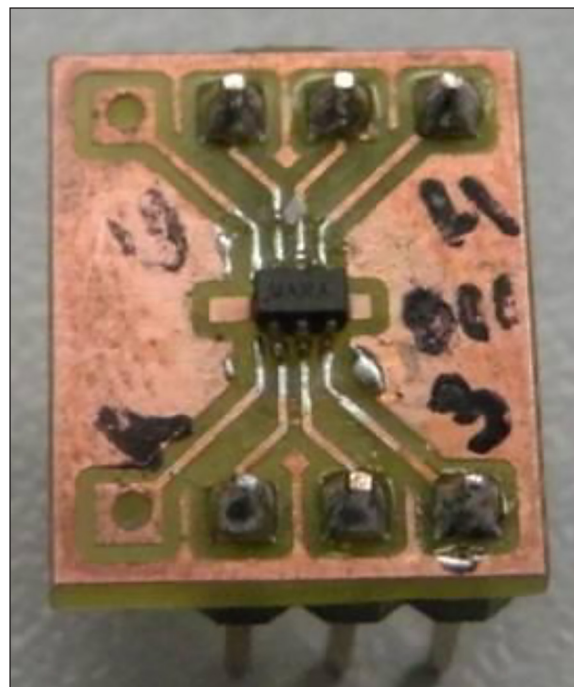


Figure 31. SIP 32431 chip

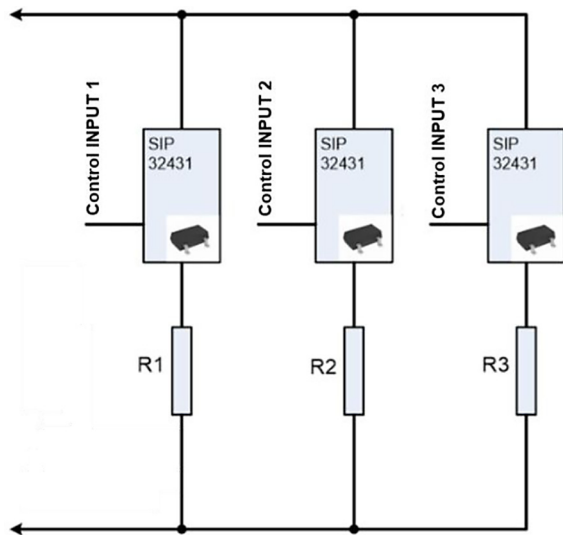


Figure 32. Diagram and control principle of the configurable load system

A digital oscilloscope was used to check the correct control waveform of the attached load. Figure 33 shows an example of a load control waveform. The segment marked t_1 (about 150 ms long) is the time to switch on the RTC circuit and wait until the voltage at the converter output after the supercapacitor reaches at least 1.8 V (in the case of tests using a linear stabiliser, this value was 1.7 V). Only then a load can be connected to the circuit under test. If the voltage at the terminals of the supercapacitor had values much higher than 1.8 V, the waiting time for the load to be connected to the system t_1 had small values, or the load was immediately connected to the system. On the other hand, when the voltage at the terminals of

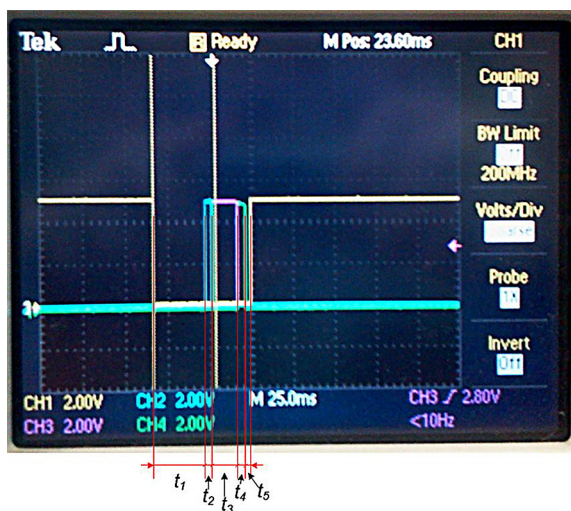


Figure 33. Control signal waveform for simulated load

the supercapacitor was below 1.8 V, the time before the load was connected increased. This was due to the need for the inverter to raise the voltage to the required value. The time t_2 is responsible for simulating the load, which in the real system is the processor initiating the entire measurement process, t_3 is the period during which the attached sensor measures the given quantity, and t_4 is the time for processing and storing the measurement data in memory. Lastly, time t_5 is the time to wait before switching off the RTC after the whole process related to the task performed by the identifier according to the scenario.

The times were determined during the execution of the measurements and $t_1 = 150$ ms, $t_2 = 2$ ms, $t_3 = 15$, $t_4 = 4$ ms and $t_5 = 2$, respectively. The resistance values placed in each branch of the circuit were, correspondingly: 5 k Ω , 20 k Ω and 2.2 k Ω .

Tests were carried out for several cases. The frequency at which the load was attached to the system under test was considered, as well as the type of supercapacitor energy conversion into usable form used. The load was attached to the system under test every 100 ms and every 1000 ms.

Figure 34 shows the characteristics of the discharge process of the supercapacitor used as a potential power source for the identifier in the assumed operating configurations. Based on the measurement results, it can be concluded that the use of a linear stabiliser as an intermediate stage to match the supercapacitor voltage to the useful value of the supply voltage of the systems connected to the identifier is not a very good solution. Despite the circuit simplicity, this results in high energy losses throughout the circuit. This affects the speed of the supercapacitor discharge process. In addition, when the voltage at the terminals of the supercapacitor drops below the stabilisation voltage, it is not possible to obtain a suitable output voltage value. These disadvantages are not present in a system equipped with a suitable voltage converter.

Figures 35a and 35b show the recorded voltage waveforms on the load when connected to the circuit every 100 ms and every 1000 ms, using an inverter and a linear stabiliser. It can be observed that the expected operating scenario of the system is only achievable under certain conditions and taking into account, on the one hand, the energy supply and, on the other, the spectrum of sensors used and their activation frequency. Ultimately, the autonomy of the operation of

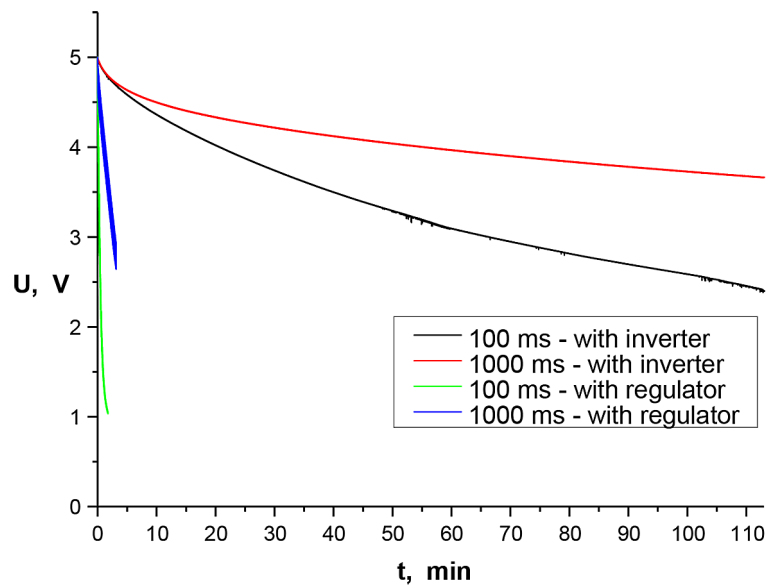


Figure 34. Voltage waveforms on a supercapacitor attached to the circuit with load connection via an inverter and linear regulator

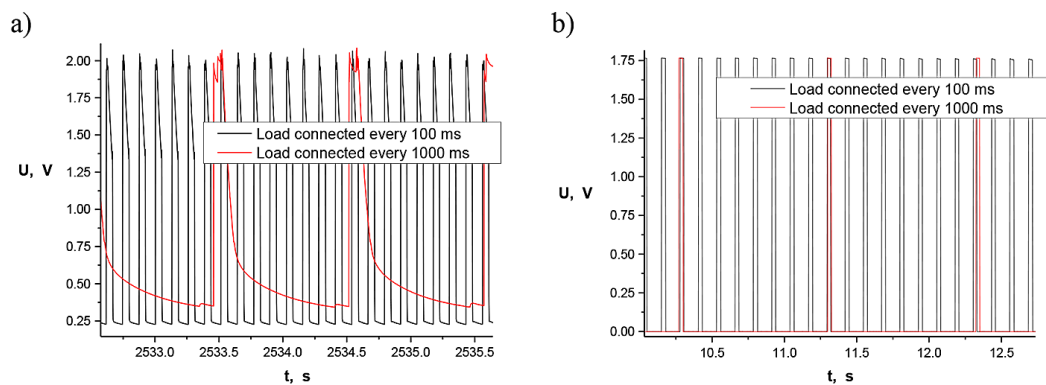


Figure 35. Voltage waveforms on the load in a system: a) with an inverter, b) with a linear regulator (stabiliser)

such a system depends anyway on the application area and the specifics of the environment in terms of the type and parameters of the available energy sources and the expectations the intensity and frequency of the system's operation. An extreme alternative, but one that may be acceptable in some situations, is to assume that the system operates only at random intervals depending on the current energy situation, accumulating energy until tripping becomes possible. It therefore becomes extremely important in this class of system to determine the energy balance of a complex system with assumptions corresponding to the required application area and to use storage with adequate capacity (the need for energy conditioning systems to the required parameter range, as well as the elimination of parasitic leakage and other losses).

CONCLUSIONS

This paper presents the results of measuring the energy harvesting efficiency from teletransmission systems of model autonomous semi-passive RFID tags. The demonstrator made as part of the research was tested two application versions. The model systems were operated under conditions corresponding to the real world, allowing these solutions to be tested for their ability to perform the energy recovery process under specific system and configuration conditions according to the developed concept of operation of the model semi-passive identifier. A suitable test stand, designed and built as part of the previous tasks, was used, allowing the tests in question to be carried out with the possibility of automatically obtaining field parameters of the electromagnetic environment close to the real one.

The detailed test results enable the characterisation of the output voltage behaviour of the harvester system under defined application conditions, including specific operational scenarios and spatial positioning relative to the electromagnetic field source utilised for energy harvesting. Additionally, they facilitate the identification of the minimum required power density levels within the intended operational environment. The measurements validate the critical importance of precise receiver tuning to the frequencies within the energy harvesting band and demonstrate the significant impact of the antenna – particularly its orientation and placement relative to the field source – on the system's performance and operating parameters.

A test stand has also been designed and built to test the identifiers for loading. On the basis of results of measurements it can be concluded that a more effective way of stabilising the supercapacitor voltage to power the identifier circuits is to use a voltage converter. It enables both higher efficiency of the entire system and allows the system to operate at much lower voltage levels as on the primary and secondary energy stores.

Finally, the obtained results make it possible to select the parameters of the identifier model system and, in particular, its operating scenario in such a way that the system for harvesting and storing energy from the electromagnetic field of common-use telecommunications systems is able to guarantee correct operation of the identifier for the desired duty cycle and expected time interval.

The identifier model system also provides for the possibility of using other additional sources of energy harvesting, such as reader-programmers of the RFID system or other sources. One of the future directions of our research in aforementioned scientific area will be investigation of the heat flux sensor module (e.g. Hukseflux FHF05SC series self-calibrating heat flux sensors with heaters) as additional source of energy harvesting.

Acknowledgments

The research leading to these results has received funding from the commissioned task entitled “VIA CARPATIA Universities of Technology Network named after the President of the Republic of Poland Lech Kaczyński” under the special purpose grant from the Minister of Education and Science, contract no. MEiN/2022/DPI/2578, as part of the action “In the neighbourhood – inter university research internships and study visits”.

REFERENCES

1. Kecik K. Experimental energy recovery from a backpack using various harvester concepts. *Advances in Science and Technology Research Journal*. 2024; 18(3): 67–78. <https://doi.org/10.12913/22998624/185848>
2. Caban J., Stączek P., Wolszczak P., Nowak R., Karczmarzyk S. Research on the use of multifrequency excitations for energy harvesting in a combustion engine. *Advances in Science and Technology Research Journal*. 2024; 18(5): 400–412. <https://doi.org/10.12913/22998624/190250>
3. Piñuela M., Mitcheson P.D., Lucyszyn S. Ambient RF energy harvesting in urban and semi-urban environments. *Trans. Microw. Theory Tech.* 2013; 61: 2715–2726. <https://doi.org/10.1109/TMTT.2013.2262687>
4. Visser H. J., Vullers R. J. M. RF energy harvesting and transport for wireless sensor network applications: principles and requirements. In: *Proceedings of the IEEE* 2013; 101(6): 1410–1423. <https://doi.org/10.1109/JPROC.2013.2250891>
5. Sardini E. and Serpelloni M. Passive and self-powered autonomous sensors for remote measurements. *Sensors* 2009; 9(2): 943–960. <https://doi.org/10.3390/s90200943>
6. Sarker M. R., Saad M. H. M., Olazagoitia J.L., Vinolas J. Review of power converter impact of electromagnetic energy harvesting circuits and devices for autonomous sensor applications. *Electronics* 2021; 10(9): 1108. <https://doi.org/10.3390/electronics10091108>
7. Digregorio G. and Redouté J. -M. Electromagnetic energy harvester targeting wearable and biomedical applications. *Sensors* 2024; 24(7): 2311. <https://doi.org/10.3390/s24072311>
8. Kim S., Vyas R., Bito J., Niotaki K., Collado A., Georgiadis A., Tentzeris M. M. Ambient RF Energy-Harvesting Technologies for Self-Sustainable Standalone Wireless Sensor Platforms. In: *Proceedings of the IEEE November* 2014; 102: 1649–1666. <https://doi.org/10.1109/JPROC.2014.2357031>
9. Radhika N., Preetika T., Prabhakar T. V., Vinoy K.J. RF Energy Harvesting For Self Powered Sensor Platform. In: *Proceedings of the 16th IEEE International New Circuits and Systems Conference (NEWCAS)*, Montreal, QC, Canada, June 2018; 148–151. <https://doi.org/10.1109/NEWCAS.2018.8585659>
10. Bakır M., Karaaslan M., Altıntaş O., Bagmancı M., Akdoğan V., Temurtaş F. Tunable energy harvesting on UHF bands especially for GSM frequencies. *International Journal of Microwave and Wireless Technologies* 2018; 10(1): 67–76. <https://doi.org/10.1017/S1759078717001325>

11. Beng L. T., Meng L. N., Kiat P. B., Kyaw T. (2014 July). Pervasive RF energy harvesting system (GSM 900 and GSM 1800). In: Proceedings of the 2014 IEEE Conference on Technologies for Sustainability (SusTech) Portland, OR, USA, 2014; 273–276. <https://doi.org/10.1109/SusTech.2014.7046257>
12. Ho D. K., Ngo V. D., Kharrat I., Vuong T. P., Nguyen Q. C., Le M. T. A novel dual-band rectenna for ambient RF energy harvesting at GSM 900 MHz and 1800 MHz. *Advances in Science Technology and Engineering Systems Journal* 2017; 2(3): 612–616.
13. Malaeb M., Tlili B. RF Energy Harvesting System for GSM900 and GSM1800 Bands. In: Proceedings of the International Conference on Renewable Energy: Generation and Applications (ICREGA), Al Ain United Arab Emirates, February 2021; 9–14. <https://doi.org/10.1109/ICREGA50506.2021.9388306>
14. Vyas R., Nishimoto H., Tentzeris M., Kawahara Y., Asami T. A battery-less energy harvesting device for long range scavenging of wireless power from terrestrial TV broadcasts. In: 2012 IEEE/MTT-S International Microwave Symposium Digest Montreal, QC, Canada, 2012; 1–3. <https://doi.org/10.1109/MWSYM.2012.6259708>
15. Vyas R. J., Cook B. B., Kawahara Y., Tentzeris M. M. E-WEHP: A batteryless embedded sensor-platform wirelessly powered from ambient digital-TV signals. *IEEE Transactions on microwave theory and techniques* 2013; 61(6): 2491–2505. <https://doi.org/10.1109/TMTT.2013.2258168>
16. Nishimoto H., Kawahara Y., Asami T. Prototype implementation of wireless sensor network using TV broadcast RF energy harvesting. In: Proceedings of the 12th ACM international conference adjunct papers on Ubiquitous computing-Adjunct, Association for Computing Machinery, New York, NY, USA, 2010: 373–374. <https://doi.org/10.1145/1864431.1864442>.
17. Olgun U., Chen C. C., Volakis J. L. Design of an efficient ambient WiFi energy harvesting system. *IET Microwaves Antennas & Propagation* 2012; 6(11): 1200–1206. <https://doi.org/10.1049/iet-map.2012.0129>
18. Hong S. S. B., Ibrahim R. B., Khir M. H. M., Zakariya M. A. B., Daud H. WI-FI energy harvester for low power RFID application. *Progress In Electromagnetics Research C* 2013; 40: 69–81. <https://doi.org/10.2528/PIERC13041608>
19. Kadir E. A., Hu A. P., Biglari-Abhari M., Aw K. C. Indoor WiFi energy harvester with multiple antenna for low-power wireless applications. In: 2014 IEEE 23rd International Symposium on Industrial Electronics (ISIE) Istanbul, Turkey, 2014; 526–530. <https://doi.org/10.1109/ISIE.2014.6864668>
20. Hong H. Cai X. Shi X. Zhu X. (2012). Demonstration of a highly efficient RF energy harvester for Wi-Fi signals. In: 2012 International Conference on Microwave and Millimeter Wave Technology (ICMMT) Shenzhen, China, 2012; 1–4. <https://doi.org/10.1109/ICMMT.2012.6230448>
21. Sabat W., Klepacki D., Kamuda K., Kuryło K., Jankowski-Mihulowicz P. Efficiency Measurements of energy harvesting from electromagnetic environment for selected harvester systems. *Electronics* 2023; 12(20): 4247. <https://doi.org/10.3390/electronics12204247>
22. Kamuda K., Klepacki D., Sabat W., Kuryło K., Skoczylas M., Jankowski-Mihulowicz P. Efficiency measurements of energy harvesting from electromagnetic environment for selected general purpose telecommunication systems. *Electronics* 2024; 13(16): 3111. <https://doi.org/10.3390/electronics13163111>
23. PN-EN 55016-2-3:2017-06/A1:2020-01, Requirements for measuring apparatus and methods for measuring radio-disturbance and resistance to disturbances - Part 2–3: Methods for measuring disturbances and testing for immunity - Measurements of radiated disturbances, 2020, Polish Committee for Standardization.
24. Product Datasheet of Evaluation Board for P2110. Available online: <https://www.powercastco.com/wp-content/uploads/2021/06/P21XXCSR-EVB-Datasheet-v2.1-1.pdf> (Accessed:15.03.2024).